Methodology for Estimation of Tissue Noise Power Spectra in Iteratively Reconstructed MDCT Data

Petr Walek
Dept. of Biomedical Engineering
Brno University of Technology
612 00, Brno, Czech Republic
walek@feec.vutbr.cz

Jiri Jan
Dept. of Biomedical Engineering
Brno University of Technology
612 00, Brno, Czech Republic
jan@feec.vutbr.cz

Petr Ourednicek
Dept. of Imaging Methods
University Hospital St. Anna,
Medical Fac. of Masaryk Uni.
656 91, Brno, Czech Republic
petr.ourednicek@philips.com

Jarmila Skotakova
Children's Hospital - Faculty Hospital
Masaryk University
625 00, Brno, Czech Republic
jskotakova@fnbrno.cz

Igor Jira
Children's Hospital - Faculty Hospital
Masaryk University
625 00, Brno, Czech Republic
igor.jira@fnbrno.cz

ABSTRACT

Iterative reconstruction algorithms have been recently introduced into X-ray computed tomography imaging. Enabling patient dose reduction by up to 70% without affecting image quality they deserve attention; therefore properties of noise present in iteratively reconstructed data should be examined and compared to the images reconstructed by conventionally used filtered back projection. Instead of evaluating noise in imaged phantoms or small homogeneous regions of interest in real patient data, a methodology for assessing the noise in full extent of real patient data and in diverse tissues is presented in this paper. The methodology is based on segmentation of basic tissues, subtraction of images reconstructed by different algorithms and computation of standard deviation and radial one-dimensional noise power spectra. Tissue segmentation naturally introduces errors into estimation of noise power spectra; therefore, magnitude of segmentation error is examined and is considered to be acceptable for estimation of noise power spectra in soft tissue and bones. As a result of this study it can be concluded that iDose^4 hybrid iterative reconstruction algorithm effectively reduces noise in multidetector X-ray computed tomography (MDCT) data. The MDCT noise has naturally different characteristics in diverse tissues; thus it is object dependent and phantom studies are therefore unable to reflect its whole complexity.

Keywords

X-ray computed tomography, iterative reconstruction, dose reduction, image quality, noise power spectra.

1 INTRODUCTION

Reduction of patient radiation dose introduced by MDCT is very topical theme nowadays as a number of examinations and thus overall population radiation exposure are steadily increasing. As a result of increased effort in this branch, modern iterative reconstruction methods have been introduced, which enable reduction of patient dose by up to 70%, declaratively without affecting image quality. Such a dramatic dose reduction is enabled by inclusion of photon counting statistics nad/or models of acquisition process into the iterative reconstruction; for further details see [BKK12] and references therein. Modern iterative reconstructions have potential to replace the conventionally used filtered back projection (FBP) algorithm; therefore, properties of iteratively reconstructed images, especially in terms of image noise, must be evaluated. Many studies dealing with problem of noise evaluation in iteratively reconstructed images have been published recently. These studies are targeted either to assessment of images acquired by scanning of artificial phantoms [MGB$^+$13] or to evaluation of small regions of interest in real patient data [MNS$^+$10]. According to [SS13], phantom studies cannot affect the whole complexity of noise in iteratively reconstructed images as the noise properties are dependent on imaged objects. A similar disadvantage has the latter approach, where only very limited portion of data from a specific (in many cases homogeneous) tissue is evaluated. This contribution aims to extend these analyses; a methodology for quantitative noise properties extraction from a whole

 ISBN 978-80-86943-74-9

complex volume of iteratively reconstructed real patient data and also from fundamental tissues separately is thus presented in this paper.

2 ACQUISITION AND RECONSTRUCTION PARAMETERS

Image data processed and analyzed in this study were acquired by a Philips Briliance 64-channel CT scanner and reconstructed by a prototype of iDose[4] reconstructor, which uses hybrid iterative reconstruction to compute image data from a set of measured projections. A large set of one hundred and thirty real patient data has been acquired during ordinary operation of a radiological center in the University Hospital Brno - Children's Medical Center. The data set is evenly distributed between males and females aged in the range from one month to eighty years and contains images of three main body parts (head, abdominal and thoracic). Each patient was scanned either with a regular dose according to the standard scanning protocol, or in the high quality mode (HQ) or with reduced radiation dose. The rate of the dose reduction was chosen according to Tab. 1 and was controlled by respective reduction of tube anode current.

Body part	Brain	Thorax	Abdomen
Reduction	0% red.	0% red.	0% red.
	30% red. HQ	30% red.	30% red.
	30% red.	70% red.	80% red.

Table 1: Choice of dose reduction while scanning diverse body parts

Acquired raw data were reconstructed once by FBP and four times by iDose[4], always with two differently adjusted reconstruction parameters. The two parameters were: ID level, which, according to [Hea], defines percentual strength of iterative reconstruction in reducing quantum noise, and Multi Resolution option, which can be activated additionally to any selected ID level. In this study, ID level was selected to be 30% (ID30), 50% (ID50) and 70% (ID70) independently on imaged body part, patient sex, age and dose reduction. Interpretation of the ID level is as follows: an image acquired with 30% dose reduction and reconstructed by iDose[4] with level ID30 is declared to have equal standard deviation of noise as the identical image acquired with full dose and reconstructed using FBP.

3 TISSUES SEGMENTATION

As already stated, the main disadvantage of many studies evaluating noise properties of iteratively reconstructed images is in the fact that these approaches can not provide comprehensive and precise description of image noise when it is spatially dependent on imaged anatomical structures (i.e. the nature of image noise is different e.g. in bones and in soft tissue). In order to overcome this problem, segmentation of basic tissues in acquired data must be done and noise properties must be evaluated separately in the segmented tissues.

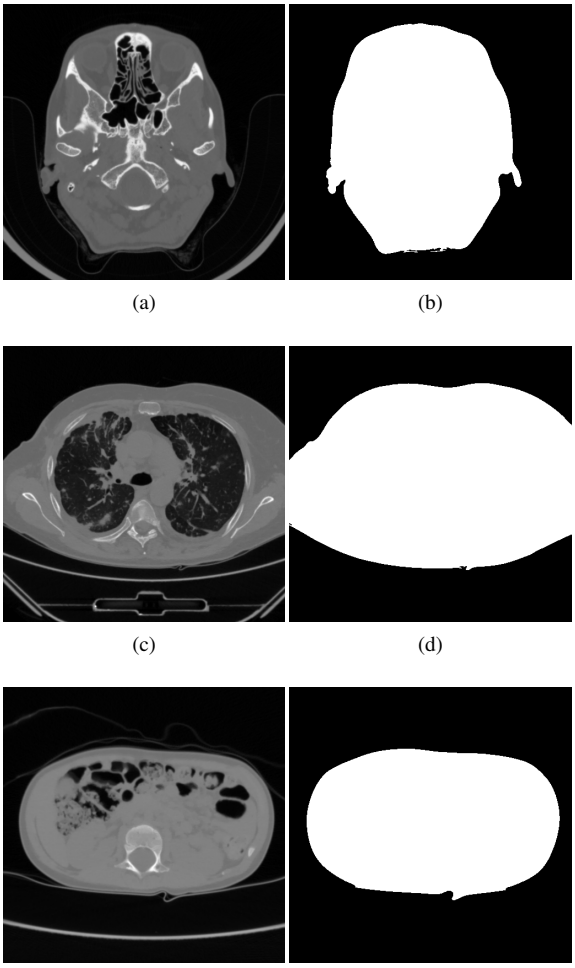

Figure 1: Examples of binary masks used for elimination of uninteresting structures computed from three main body parts: (a) slice of original brain data, (b) mask computed from (a), (c) slice of original thoracic data, (d) mask computed from (c), (e) slice of original abdominal data, (f) mask computed from (e).

The segmentation is based on our methodology previously published in [WJ12] where distinguishing between fundamental tissues is carried out by thresholding and subsequent classification of insufficiently segmented trabecular bones. In order to make the paper self-explaining, the methodology of the segmentation algorithm is briefly presented; however, interested readers are referred to [WJ12] for further details.

Although thresholding is conceptually very simple, a problem is in proper determination of thresholds for distinguishing between tissues, especially when

 ISBN 978-80-86943-74-9

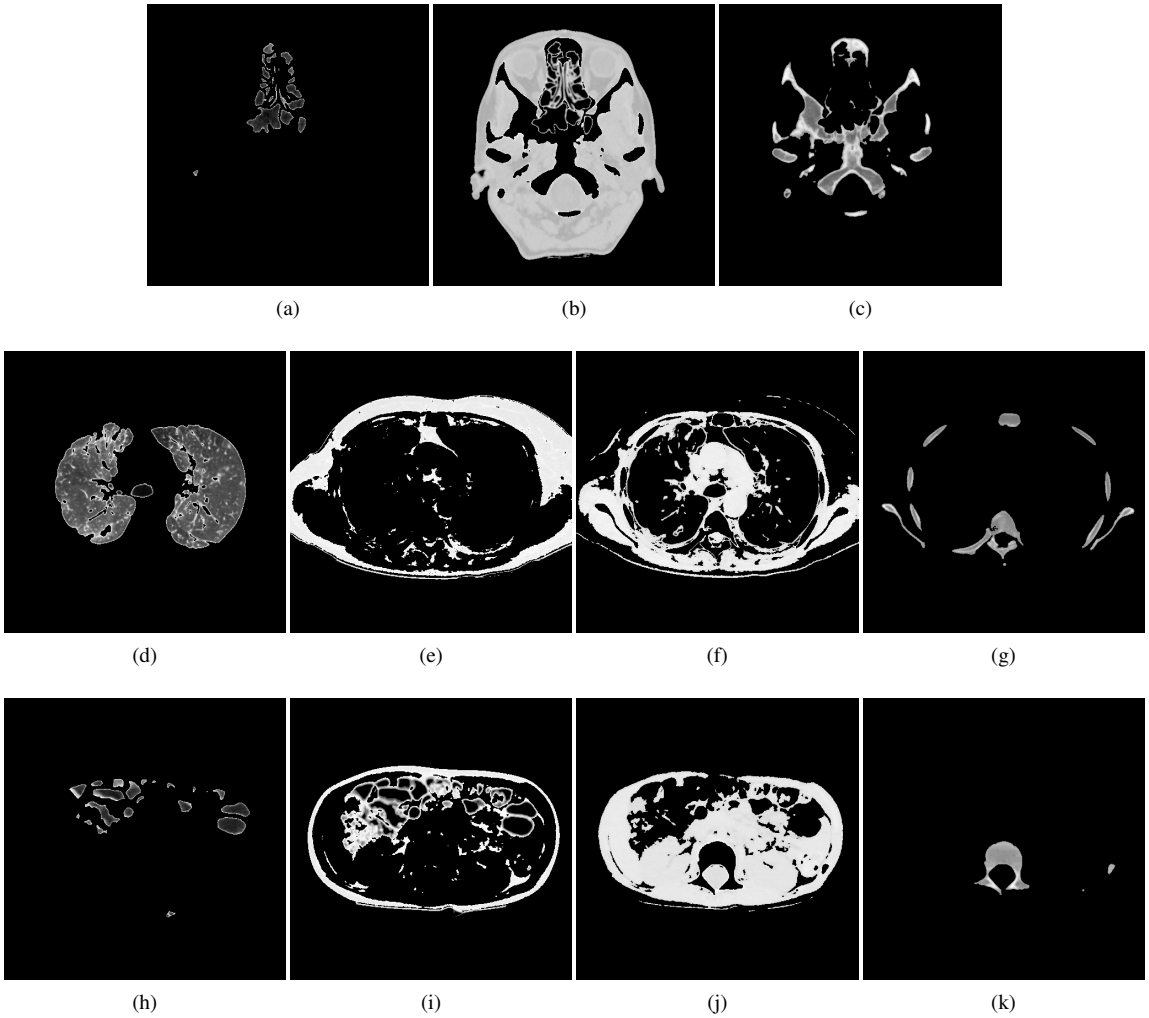

Figure 2: Images resulting from segmentation of brain 1a (a) - (c), thoracic 1c (d) - (g) and abdominal 1e (h) - (k) data: Segments of brain image are (a) paranasal sinuses, (b) soft tissue and (c) bones. Segments of thoracic image are (d) lungs, (e) adipose tissue, (f) soft tissue, (g) bones. Segments of abdominal image are (h) air in colon, (i) adipose tissue, (j) soft tissue, (k) bones.

acquired data vary substantially between imaged body parts and also within the scope of specific body part as a result of different patient age, sex, body proportions, pathologies etc. Evaluation of grayscale histogram is used to solve this problem, as histograms of the body parts are characterized by several very apparent peaks (e.g. a typical histogram of thoracic body part contains four peaks, which are representations of surrounding air, lung, adipose tissue and soft tissue). By a peak detection algorithm, one-dimensional linear and median filtering, applied consecutively on histograms, only significant peaks are detected. Positions and magnitudes of detected peaks serve as parameters of initial Gaussian curves, which are then optimally fitted to the histogram using least-squares method, and final thresholds for segmentation are subsequently determined from those optimally fitted curves.

Due to overlapping of Hounsfield units (HU) of soft tissue and inner parts of bones (trabecular bones), thresholding is unable to distinguish exactly between them. The imperfect segmentation of bones causes areas of zeros fully surrounded by ones in binary images representing segmentation of bones, which are extracted using a boundary tracking algorithm. The extracted areas represent either trabecular bones or soft tissue. Although the Hounsfield units of soft tissue and trabecular bones are partially overlapping, the shapes of their histograms differ substantially thanks to apparent texture of trabeculae in inner part of bones. In contrast with soft tissue histograms, the histograms of trabecular bones are more compact and skewed towards higher Hounsfield units. The shape differences are quantified by four parameters; entropy, compactness, skewness and kurtosis, so that each area is described by a feature vector of those parameters. The final step in segmen-

 ISBN 978-80-86943-74-9

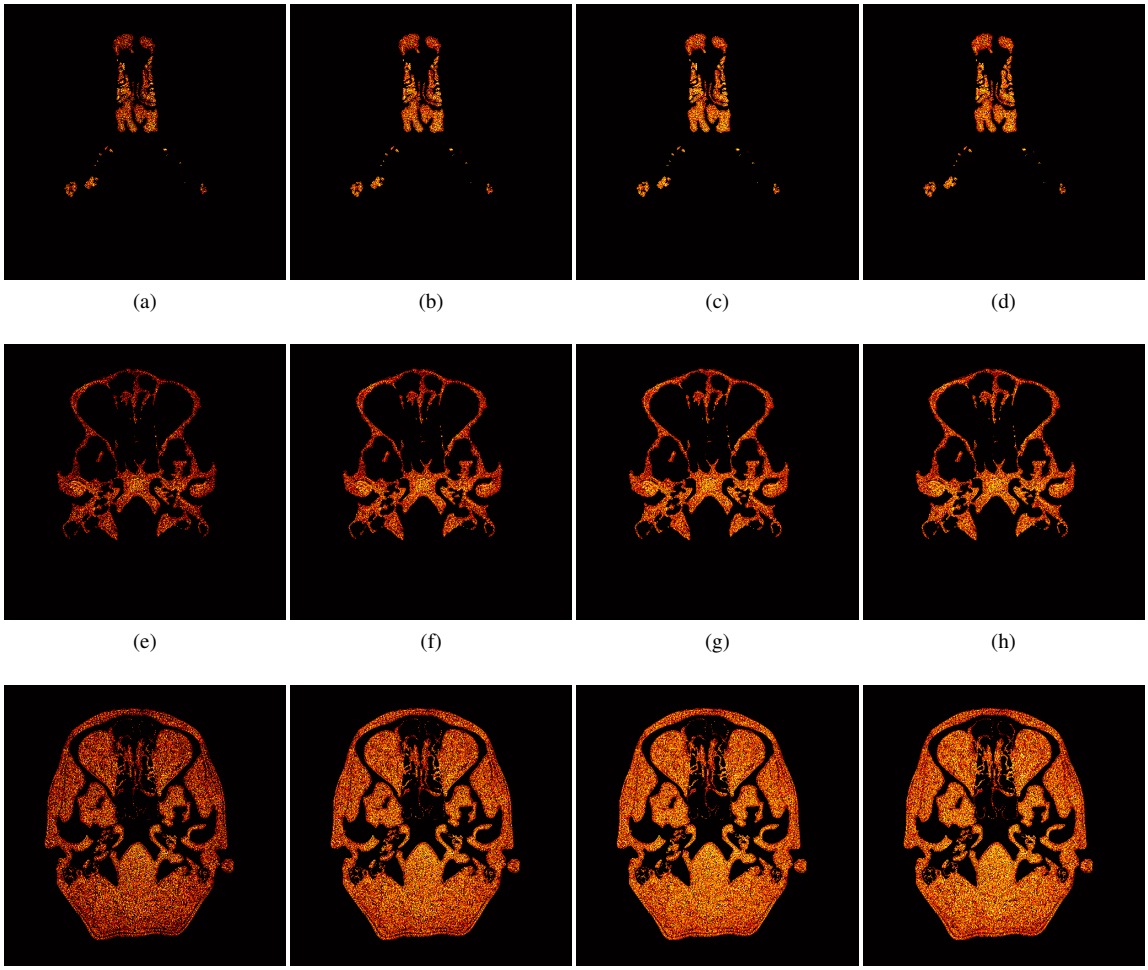

Figure 3: Residual noise images of a head body part: (a) - (d) residual noise images of paranasal sinuses, (e) - (h) residual noise images of bones, (i) - (l) residual noise images of soft tissue. First column - subtraction of ID30 and FBP reconstruction, Second column - subtraction of ID50 and FBP reconstruction, third column - subtraction of ID70 and FBP reconstruction, fourth column - subtraction of ID70MR and FBP reconstruction. The residual noise images are depicted in absolute value and logarithmic scale for highlighting small differences between them.

tation is the decision, whether extracted areas represent soft tissue or trabecular bone, based on these vectors classified by an artificial neural network.

The described segmentation algorithm is slightly modified in this paper as only noise parameters inherent to tissues of human body should be assessed. Acquired images contain also unimportant structures, such as surrounding air and patient table, which must be removed prior to applying the described segmentation. Removing of unimportant structures is performed in three simple steps. The first step is thresholding using a threshold determined by Otsu method [Ots79], which optimally distinguish between objects and background. The background involves surrounding air and low density tissues such as lung or paranasal sinuses, whereas the foreground is formed by tissues of human body and the metallic part of patient table. Connected binary segments of foreground are labeled and size of each segment is computed. Providing that the largest connected binary segment represents the human body (it is always true for our data set), other foreground structures are removed by binary area opening [Soi03]. The last step is addition of interesting structures from background (typically sinuses and lungs) to the final binary mask. With respect to continuity of human body, organs filled by air must be surrounded by tissue, and the addition can be performed by filling based on morphological reconstruction [Soi03]. Examples of binary masks used for elimination of uninteresting structures are depicted in Fig. 1 together with corresponding slices of original data. Final segmentations of basic tissues, carried out on original images depicted in Fig. 1, are presented in Fig. 2, where binary masks resulting from the segmentation are multiplied with corresponding original data.

 ISBN 978-80-86943-74-9

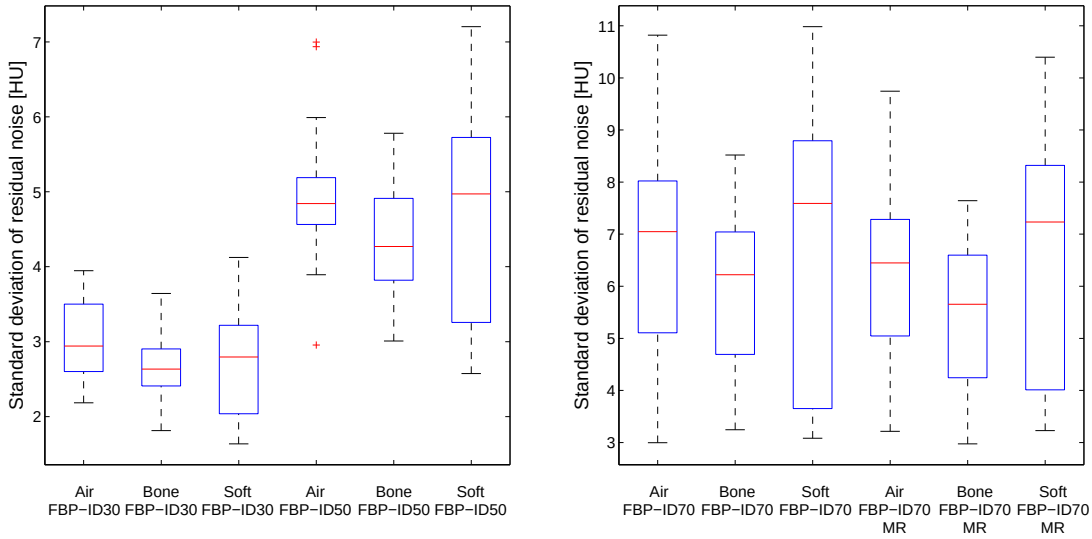

(a) (b)

Figure 4: Box plots of residual noise standard deviations, computed from whole set of patient data, in dependence on ID level and imaged tissue. The central red line is a median, blue horizontal edges of box are 25th and 75th percentiles, dashed lines cover extent of the most extreme points and red crosses indicate outliers.

4 RESIDUAL NOISE IMAGES AND NOISE DESCRIPTORS

In order to compare noise properties of images reconstructed by iDose[4] with images reconstructed by FBP, the anatomical structures must be removed and images of pure noise must be analyzed. Images obtained by FBP and by iDose[4] are reconstructed from a single set of raw data (for a single patient); they are therefore in perfect spatial coherence and they can be subtracted without further registration. Providing that anatomical information is identical in every reconstruction, images of pure noise are obtained by subtraction of data reconstructed using FBP from the iteratively reconstructed data (i.e. data labeled by ID30, ID50, ID70 and ID70MR). They are called residual noise images and are subject of further analysis. According to [BCK+04], head images do not contain any structures likely to produce streaking artifacts; therefore their residual noise images contain only the statistical noise, which is easier to analyze. Hence, only head residual noise images will be analyzed in this paper. Binary masks resulting from the proposed segmentation are multiplied with residual noise images, see Fig. 3, so that noise properties can be evaluated in diverse tissues separately.

4.1 Standard deviation

The standard deviation (STD) provides fundamental information about the degree of statistical noise in images acquired using MDCT. Interpretation of residual noise STD is rather complicated, when taking into the account that subtraction of two random fields (i.e. noise realizations in images reconstructed by FBP and iDose[4]) results in a new random field with a different STD. In [WJO+12] it is shown that STD of residual noise indicates the relative improvement of noise standard deviation in an iteratively reconstructed image with respect to the correcponding image reconstructed by FBP. Box plots, calculated from the whole set of 40 brain images, showing standard deviations of residual noise as dependent on ID level and tissue type are depicted in Fig. 4. A rising trend of residual noise STD in dependence on ID level can be observed, which according to [WJO+12] indicates lover content of noise in images reconstructed with higher ID level. Fig. 4 also provides evidence of spatial variance of noise as the STD is different in diverse tissues.

4.2 Radial 1D noise power spectra

Even though STD is a valuable measure of statistical noise in MDCT images, it provides information only about average magnitude of image noise; however, its frequency distribution is very important for human perception. Such information may be obtained by computation of noise power spectrum (NPS), which is often used as a quality measure of MDCT imaging systems [BCMG07], [BNCL09]. A direct digital method for computation of NPS presented in [SCJ02] and [YKH+08] and expressed as

$$\mathbf{S}(f_x,f_y) = \frac{b_x b_y}{L_x L_y} \cdot \left\langle \left| DFT_{2D}\left\{\mathbf{D}(x,y) - \mathbf{D}_{\mathbf{filt}}(x,y)\right\}\right|^2 \right\rangle \quad (1)$$

is used. Each slice of a 3D residual noise matrix, which is considered to be one realization of a stochastic field (i.e. stochastic image), is denoted as $\mathbf{D}(x,y)$ and must

 ISBN 978-80-86943-74-9

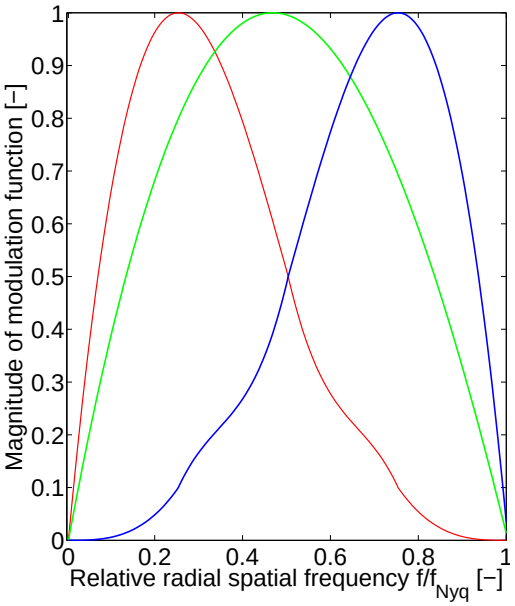

Figure 5: One dimensional functions designed for modulation of white noise spectra: (|) simulation of low frequency noise, (|) simulation of mid frequency noise, (|) simulation of high frequency noise.

be locally zero mean detrended prior to computation of NPS; hence subtraction of image filtered by a low pass Gaussian filter $\mathbf{D_{filt}}(x,y)$ is performed. The individual power spectrum of a noise realization is computed by squaring absolute value of 2D Fourier transform of the detrended noise realization. As individual noise power spectra suffer from large fluctuations between realizations, power spectrum of the stochastic field (i.e. the process generating random noise) must be computed as mean value of individual noise power spectra (outlined by $\langle\circ\rangle$ operator). Normalization by sampling periods b_x, b_y and image sizes L_y, L_x in directions x and y, respectively, must be done to enable comparison of power spectra of different stochastic fields. 2D NPS computed according to equation (1) is a comprehensive descriptor of noise frequency distribution; nevertheless, it is rather complicated to evaluate or extract some descriptive parameters from it. Providing that 2D NPS is rotationally symmetric, it can be expressed by radial (one-dimensional) noise power spectrum without any loss of information [BNCL09]. The radial 1D noise power spectrum is computed by angular averaging of 2D noise power spectrum and therefore is a function of the absolute spatial frequency

$$f = \sqrt{f_x^2 + f_y^2}. \tag{2}$$

Equation (1) assumes that the noise matrix $\mathbf{D}(x,y)$ is fully filled with measured noise; however, this premise is not fulfilled in case of segmented residual noise images, since they contain many zero pixels not contributing to computation of 2D NPS, see Fig. 3. Normalization of 2D NPS must therefore be reformulated and equation (1) is changed to

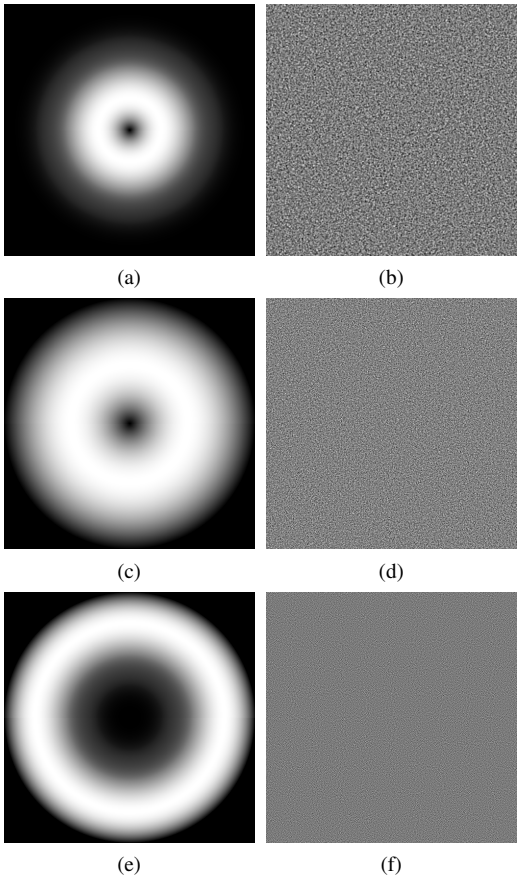

Figure 6: Two dimensional modulation functions and slices from simulated colored noise: Functions for (a) low, (c) mid and (e) high frequency noise. Examples of simulated (b) low, (d) mid and (f) high frequency noise.

$$\mathbf{S}(f_x,f_y) = \frac{b_x b_y}{L_B} \cdot \left\langle \left| DFT_{2D}\left\{\mathbf{D}(x,y) - \mathbf{D}_{filt}(x,y)\right\}\right|^2 \right\rangle, \tag{3}$$

where the normalization term L_B correspond to total count of pixels contributing to computation of 2D NPS. L_B can be computed as sum of pixels of the corresponding binary segmentation mask $\mathbf{B}$.

$$L_B = \sum_{x=1}^{L_x}\sum_{y=1}^{L_y} \mathbf{B}(x,y) \tag{4}$$

As stated before, multiplying binary masks resulting from segmentation with residual noise images is necessary; however it inevitably introduces error to estimation of NPS. According to convolutional property of Fourier transform (equation (5) [Jan06]), multiplication of two signals in the original domain corresponds to convolution of their spectra in the spectral domain.

$$FT\{f(x,y)g(x,y)\} = \frac{1}{4\pi^2} F(f_x,f_y) {}^{*} G(f_x,f_y) \tag{5}$$

 ISBN 978-80-86943-74-9

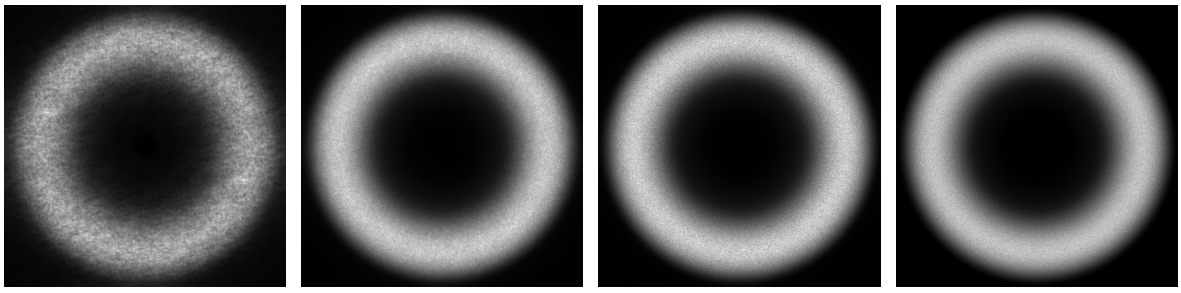

(a) (b) (c) (d)

Figure 7: Two dimensional NPS computed from simulated high frequency noise multiplied with various binary segmentation masks of: (a) paranasal sinuses, (b) bones, (c) soft tissue and (d) full noise matrix.

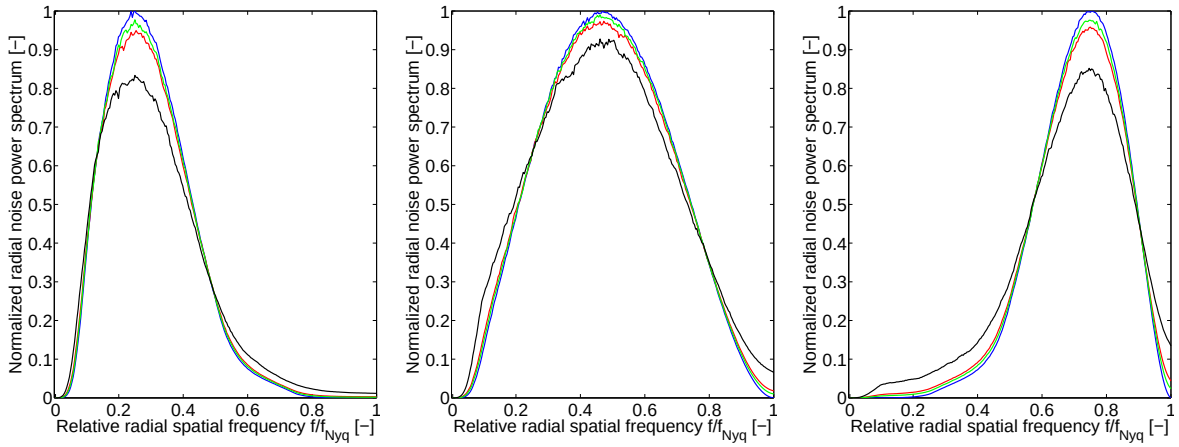

(a) (b) (c)

Figure 8: One dimensional NPS computed from (a) low, (b) mid and (c) high frequency noise multiplied with various binary segmentation masks of: (|) paranasal sinuses, (|) bones, (|) soft tissue and (|) full noise matrix.

The NPS of residual noise estimated by equation (3) is therefore a convolution of the sought noise power spectrum and the spectrum of a weighting binary mask, and this causes errors in estimation of 2D- and consequently of radial 1D noise power spectrum. Magnitude of the error must be evaluated prior to computation of 1D NPS of a real patient data.

4.2.1 Simulation of MDCT noise

To be able to compute errors of 1D NPS estimation caused by segmentation, three simulated matrices sized $512 \times 512 \times 512$ voxels filled with zero-mean white noise and standard deviation 10 are generated. The statistical noise inherent to MDCT images is not typically white [BCMG07]; therefore the generated model noise need to be colored (its spectral envelope must be modulated). One dimensional modulation functions based on cubic Bézier curves, see Fig.5, are designed to simulate low, mid and high frequency noise and subsequently rotationally extended to two dimensional functions MOD_{2D}. Coloring of the 3D white noise matrix is undertaken in frequency domain according to equation 6 applied slice by slice. Finally, the required 3D colored noise matrix N_{Col} is obtained,

$$N_{Col} = IDFT_{2D}\{DFT_{2D}\{N_{White}\} \cdot MOD_{2D}\}. \qquad (6)$$

In Fig. 6, the 2D modulation functions can be seen together with slices taken from simulated colored noise matrices.

4.2.2 Segmentation error of radial 1D NPS

The simulated noise matrices have their noise power spectra defined by the modulation functions and thus the segmentation error of 1D NPS estimation can be evaluated. Data acquired from head body part are segmented (data reconstructed by ID70 are used as they contain the lowest portion of noise) and the three resulting binary masks (representing paranasal sinuses, bones and soft tissue) are multiplied with each of the three matrices containing low, mid and high frequency noise. Nine weighted noise matrices are together with three full noise matrices subjects of 2D- and 1D NPS computation according to equation (3). Examples of estimated 2D NPS can be seen in Fig. 7, while Fig. 8 shows 1D NPS computed from each binary mask and from low, mid and high frequency noise matrices.

 ISBN 978-80-86943-74-9

	Low		Mid		High	
	Mean	Std	Mean	Std	Mean	Std
Bone	2.8	2.9	3.0	2.0	3.7	2.8
Sinuses	5.2	5.4	5.8	3.7	7.0	5.1
Soft	0.8	0.81	0.82	0.51	1.0	0.72

Table 2: Mean value and standard deviations of percentage segmentation errors.

The errors of 1D NPS estimation introduced by segmentation of tissues are computed as absolute value of differences between the estimated 1D NPS using a binary segmentation mask and the 1D NPS of full noise matrix. The errors are computed for the whole 40 patients data set and the resulting mean values and standard deviations of the errors are summarized in table 2.

The dependences of the segmentation errors on absolute spatial frequency are visualized by box plots in Fig.9, the visualization of error computed on the high frequency noise is chosen as the worst case according to table 2. The mean values and standard deviations of the errors are varying with the absolute spatial frequency. Comparing plots in Fig. 9 with the blue plot in Fig. 5, reveals that they are obviously dependent on shape of the estimated 1D NPS.

4.2.3 1D NPS of real patient data

Finally, noise power spectra of residual noise matrices in their 2D- and radial 1D forms can be computed according to equation (3) and thanks to mentioned segmentation algorithm, in each of the fundamental tissues separately. Examples of 2D NPS computed from residual noise images (FBP minus ID70) are depicted in Fig. 10 while examples of 1D NPS computed from diverse residual noise images and diverse tissues (i.e. the set of images depicted in Fig. 3) can be seen in Fig. 11.

5 CONCLUSIONS AND FUTURE WORK

A methodology for computation of radial 1D noise power spectra separately in diverse tissues of iteratively reconstructed CT image data is presented in this paper. Thanks to fully automatic segmentation algorithm and subtraction of images reconstructed by different algorithms, pure noise images representing noise inherent to fundamental tissues (called residual noise images) are obtained. Analyzing standard deviations of the residual noise images one can conclude that iterative reconstruction with higher ID level produces images with lower content of statistical noise compared to the one with lower ID level. A further deeper statistical analysis is needed to relate the improvement in suppression of image noise introduced by the iterative reconstruction to the chosen dose reduction, patient weight etc.

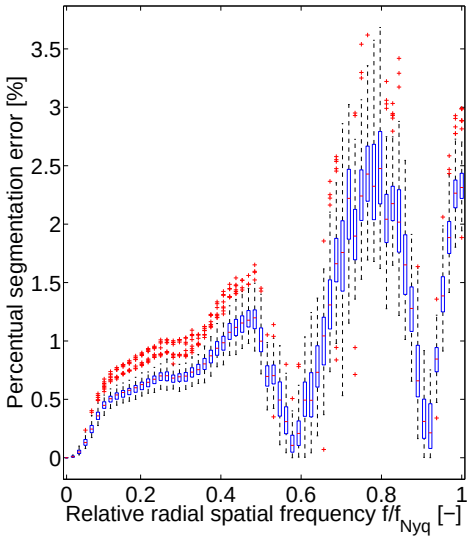

(a)

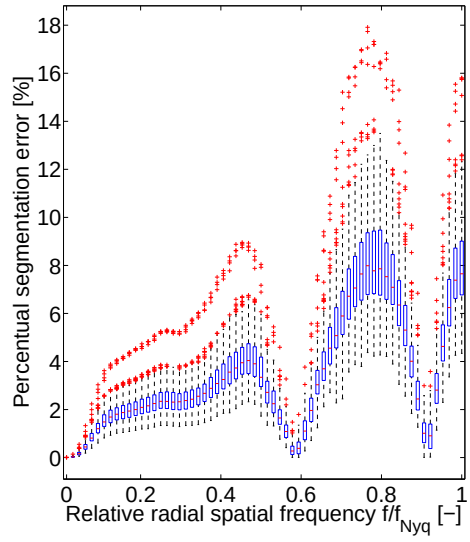

(b)

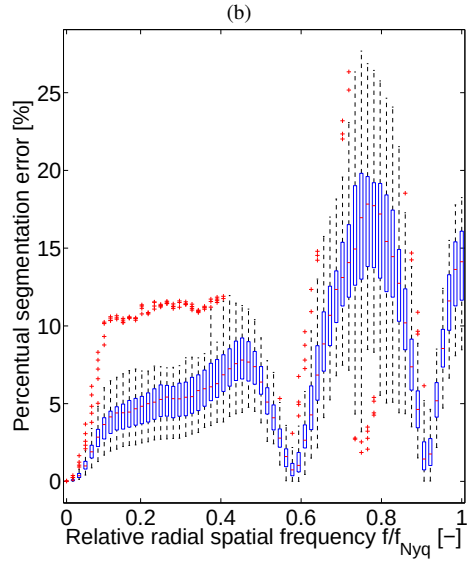

(c)

Figure 9: Box plots of errors in 1D NPS estimation introduced by segmentation of: (a) soft tissue, (b) bones, (c) paranasal sinuses.

 ISBN 978-80-86943-74-9

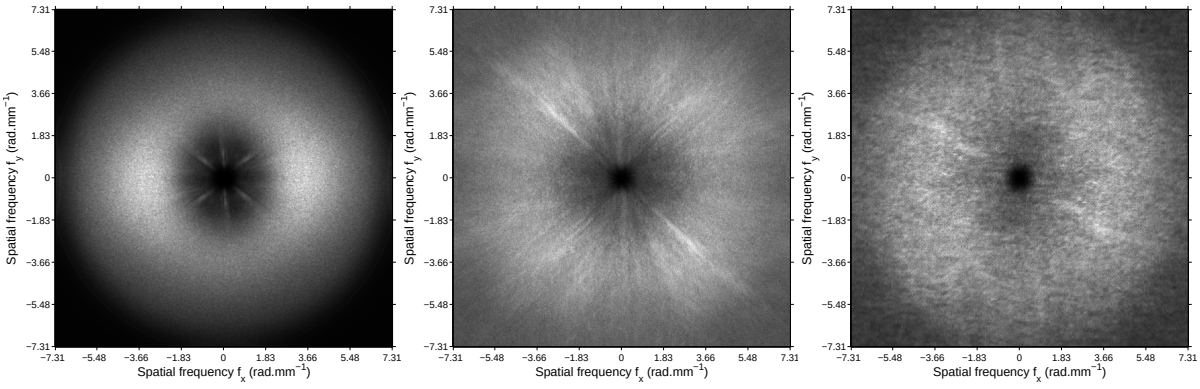

(a) (b) (c)

Figure 10: 2D NPS of real patient data representing frequency characteristic of noise inherent to: (a) soft tissue, (b) bones and (c) paranasal sinuses.

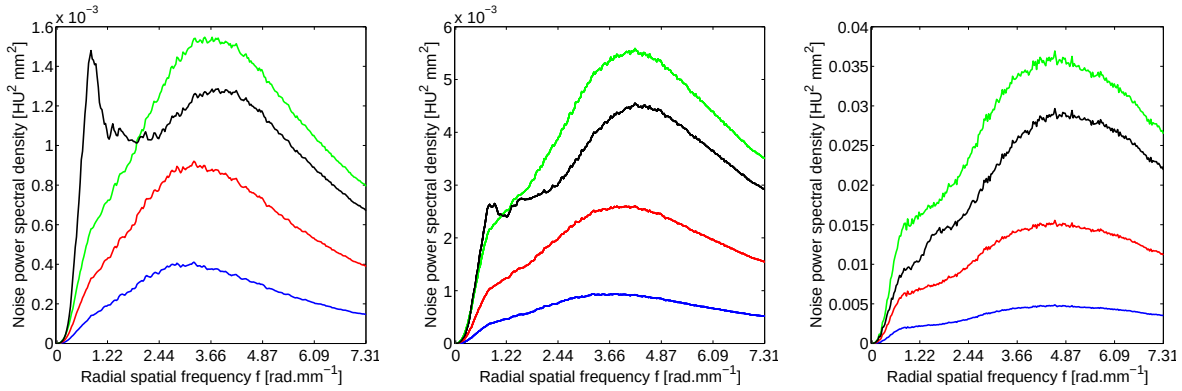

(a) (b) (c)

Figure 11: 1D NPS o real patient data representing frequency characteristic of noise inherent to: (a) soft tissue, (b) bones and (c) paranasal sinuses. Each plot shows four 1D NPS curves computed from diverse residual nose images: (|) FBP minus ID30, (|) FBP minus ID50, (|) FBP minus ID70 and (|) FBP minus ID70MR.

The second parameter extracted from residual noise images is radial 1D NPS. The classical equation for 1D NPS estimation is modified to fit the character of masked residual noise images as they contain many zero elements. Estimation of 1D NPS is burdened by errors as multiplying of a noise matrix with a binary segmentation mask in the original domain results in convolution of the noise spectrum with spectrum of the segmentation mask. Errors introduced by segmentation are evaluated, and if has been found that the mean value and standard deviation of errors depend on the segmented body part as well as on the frequency content of image noise, and so on the shape of estimated noise power spectra, see box plots in Fig. 9. The examined data exhibit acceptable 1D NPS estimation error in case of soft tissue (mean value of the error is under 1%) and bones (mean value of the error is under 4%). Mean value of the error of 1D NPS estimation inherent to paranasal sinuses is under 7%, and according to Fig. 9, the error can be higher even than 25%; therefore the estimation of 1D NPS inherent to paranasal sinuses produces inacceptable results.

This type of error is well known from 1D signal processing, where shortening of theoretically infinite signal (by a rectangular temporal window) causes a decrease in frequency resolution in the spectral domain as the spectrum of weighting function (sinc function) is convoluted with each discrete frequency. This effect is often referred to as spectral leakage and may be suppressed either by prolonging the weighting window or using a window with better spectral properties. Binary masks for segmenting a soft tissue have the biggest spatial extent, which explains their lowest segmentation error. As a binary weighting mask can be considered a 2D function of variable shape with steep boarders, reduction of a segmentation error can be done by replacing the binary mask by a spatially variable two dimensional windowing function with better spectral properties (i.e. Hann or Hamming weighted) in our future work. A possibility for reducing the segmentation error is in careful exploration of outliers in box plots presented in Fig. 9, and in finding, which features of binary masks cause such large segmentation errors. Segmentation errors in form of small misclassified regions can represent one of

 ISBN 978-80-86943-74-9

the possible reasons and its influence will be explored in our future work.

As can be seen from Fig. 10, the 2D NPS of soft tissue exhibit evident rotational asymmetry in the limited range of absolute spatial frequencies. Rotationally symmetric 2D NPS is a basic assumption to proper calculation of radial 1D NPS, hence sources of the asymmetry should be found and eliminated.

Comparing the 1D NPS depicted in Fig. 11 mutually, it can be concluded that the iDose^4 generally preserves shape of the 1D NPS regardless of the used ID level. An exception can be seen in case of reconstruction with enabled Multi Resolution option, which exhibits a different shape of 1D NPS at low frequencies and a very high dependence on the imaged tissue. The 1D NPS also shows a dependence on the imaged scene as centroids of curves are apparently shifted along the frequency axis for different tissues.

Our future work will be focused on deriving parameters describing properties of 1D NPS inherent to diverse tissues and iDose reconstructions with varying ID level. A certain drawback of this method is the fact that extracted noise power spectra are, thanks to the subtraction, a mixture of spectral properties of iteratively- and by FBP- reconstructed images. Thus it is not clear, what does the NPS of residual noise really express. A phantom study revealing how the 1D NPS of residual noise is connected with the real noise power spectra of iteratively reconstructed image must be therefore done. The described methodology will be extended also to other body parts where problems with streaking artifacts, which can not be evaluated by NPS, must be solved. The residual noise images should be then divided into areas of statistical noise, which can be evaluated using the proposed methodology, and areas corresponding to streaking artifacts which must be addressed by a different methodology.

6 ACKNOWLEDGMENTS

Lending of the iDose^4 reconstructor prototype software package from Philips Healthcare is highly acknowledged as well as the long term data acquisition enabled by the Clinic of Radiology, Brno Faculty Hospital - Children's Hospital.

7 REFERENCES

[BCK+04] A. J. Britten, M. Crotty, H. Kiremidjian, A. Grundy, and E. J. Adam. The addition of computer simulated noise to investigate radiation dose and image quality in images with spatial correlation of statistical noise: an example application to X-ray CT of the brain. *British Journal of Radiology*, 77(916):323–328, April 2004.

[BCMG07] K. L. Boedeker, V. N. Cooper, and M. F. McNitt-Gray. Application of the noise power spectrum in modern diagnostic MDCT: part I. Measurement of noise power spectra and noise equivalent quanta. *Physics in medicine and biology*, 52(14):4027–46, 2007.

[BKK12] Marcel Beister, Daniel Kolditz, and Willi A. Kalender. Iterative reconstruction methods in X-ray CT. *Physica medica*, 28(2):94–108, April 2012.

[BNCL09] Ricardo Betancourt Benítez, Ruola Ning, David Conover, and Shaohua Liu. NPS characterization and evaluation of a cone beam CT breast imaging system. *Journal of X-ray science and technology*, 17(1):17–40, January 2009.

[Hea] Philips Healthcare. idose^4 iterative reconstruction. *Philips Healthcare Whitepaper. Available via https://www.healthcare.philips.com/pwc_hc/main/shared/Assets/Documents/ct/idose_white_paper_452296267841.pdf. Accessed March 2013.*

[Jan06] Jiri Jan. *Medical image processing, reconstruction and restoration: concepts and methods*. Taylor & Francis, Boca Raton, 2006.

[MGB+13] Frédéric A. Miéville, François Gudinchet, Francis Brunelle, François O. Bochud, and Francis R. Verdun. Iterative reconstruction methods in two different MDCT scanners: physical metrics and 4-alternative forced-choice detectability experiments–a phantom approach. *Physica medica*, 29(1):99–110, January 2013.

[MNS+10] Daniele Marin, Rendon C. Nelson, Sebastian T. Schindera, Samuel Richard, Richard S. Youngblood, Terry T. Yoshizumi, and Ehsan Samei. Low-tube-voltage, high-tube-current multidetector abdominal CT: improved image quality and decreased radiation dose with adaptive statistical iterative reconstruction algorithm–initial clinical experience. *Radiology*, 254(1):145–53, January 2010.

[Ots79] Nobuyuki Otsu. A Threshold Selection Method from Gray-Level Histograms. *IEEE Transactions on Systems, Man and Cybernetics*, 9(1):62–66, 1979.

[SCJ02] J. H. Siewerdsen, I. A. Cunningham, and D. A. Jaffray. A framework for noise-power spectrum analysis of multidimensional images. *Medical Physics*, 29(11):2655, 2002.

[Soi03] Pierre Soille. *Morphological image analysis*. Springer Verlag, Berlin, 2003.

[SS13] Justin Solomon and Ehsan Samei. Are uniform phantoms sufficient to characterize the performance of iterative reconstruction in CT? In *Proc. SPIE 8668, Medical Imaging 2013: Physics of Medical Imaging*, March 2013.

[WJ12] Petr Walek and Jiri Jan. Segmentation of basic tissues for assessing noise in iteratively reconstructed MDCT data. In *Advances in Sensors, Signals, Visualization, Imaging and Simulation*, pages 211–216. WSEAS Press, 2012.

[WJO+12] Petr Walek, Jiri Jan, Petr Ourednicek, Jarmila Skotakova, and Igor Jira. Preprocessing for Quantitative Statistical Noise Analysis of MDCT Brain Images Reconstructed Using Hybrid Iterative (iDose) Algorithm. In *Journal of WSCG*, volume 20, pages 73–80, Pilsen, 2012.

[YKH+08] Kai Yang, Alexander L. C. Kwan, Shih-Ying Huang, Nathan J. Packard, and John M. Boone. Noise power properties of a cone-beam CT system for breast cancer detection. *Medical Physics*, 35(12):5317, 2008.